Steady-State Electrocatalytic Activity Evaluation with the Redox Competition Mode of Scanning Electrochemical Microscopy: A Gold Probe and a Boron-Doped Diamond Substrate

Olivier Henrotte, Alice Boudet, Ndrina Limani, Philippe Bergonzo, Bacem Zribi, Emmanuel Scorsone, Bruno Jousselme, Renaud Cornut

Steady state electrocatalytic activity evaluation with the redox competition mode of SECM: the interests of a gold probe and a boron doped diamond substrate

Olivier Henrotte [a], Alice Boudet [a], Ndrina Limani [a], Philippe Bergonzo [c], Bacem Zribi [b], Emmanuel Scorsone [b], Bruno Jousselme [a] and Renaud Cornut [a]

[a] Dr. O. Henrotte, A. Boudet, N. Limani, Dr. B. Jousselme, Dr. R. Cornut
Université Paris-Saclay, CEA, CNRS, NIMBE, LICSEN
CEA Saclay 91191, Gif-sur-Yvette Cedex (France)

[b] Dr. B. Zribi, Dr. E. Scorsone
Diamond Sensors Laboratory, LIST, CEA
CEA Saclay 91191, Gif-sur-Yvette Cedex (France)

[c] Dr. P. Bergonzo
Formerly [b], now at:
Department of Electronic and Electrical Engineering, University College London
17-19 Gordon Street, London, WC1H 0AH, United Kingdom

Abstract

In the current context of energetic transition, investigations of alternative complex systems require tools as scanning electrochemical microscopy (SECM) offering interesting opportunities as an electroanalytical technique to evaluate innovative catalysts. Herein, we demonstrate how a judicious choice of probe and substrate materials opens up improved performances to achieve steady state measurements for oxygen reduction reaction (ORR) catalytic activity detection through the redox competition scanning electrochemical microscopy (RC-SECM).

On the probe side, we show that using gold enhances the stability of the local oxygen concentration detection in comparison to the regularly used platinum one. On the substrate side, we evaluate boron doped diamond as an appealing alternative to classical support substrate, that shows a low ORR activity, high stability and very good reusability.

This work introduces an alternative approach for quantitative measurements with SECM, improving measurement easiness, comfort and reproducibility, thus paving the way towards standardized benchmarking and numerical simulation-based parameter extraction.

Introduction

The global energetic transition requires innovative tools enabling the evaluation of alternative materials and systems as candidates to perform energy. Fuel cells, and proton exchange membranes, for instance, are envisioned to play a key role as an efficient alternative technology. They are considered worldwide with high interests and could be easily adopted. However, the variety of catalysts presently under consideration by the community generates a high demand to enable their comparative characterization. Improved tools would help in their discrimination[1,2]. Presently characterization methods are the limiting part of innovation and improvements, particularly when active carbon based nanomaterials are concerned[3]. During the past decades, local probe techniques, such as scanning electrochemical microscopy (SECM) have made great progress. SECM already provides impressive results in the investigation of local electrochemical properties[4]. SECM is an electroanalytical tool that consists of a four-electrodes setup: two working electrodes (WE), namely a micrometric probe as an electrochemical sensor and a substrate to polarize the investigated material, a counter electrode (CE) and a reference electrode (RE). A potential can be applied on both the probe and the substrate while the probe is moved in the close vicinity of the substrate. The versatility of the technique allows it to be used in many different fields such as electrocatalysis[5,6], corrosion[7], photo-electrochemistry[8] or even DNA detection[9] or archaeological remains investigations[10].

In the global research context of energetic transition, SECM has been used for the investigation of materials involved in energy related systems (batteries[11], solar cells[12], supercapacitors[13], etc…), in particular for fuel cells (e.g. direct methanol fuel cell[14], polymer electrolyte fuel cell[15], proton exchange membrane fuel cell (PEMFC)[16–18], etc…). The investigations here mainly focus on hydrogen evolution reaction (HER)[19] and more particularly on oxygen reduction reaction (ORR)[6,16,20] due to its slow kinetics, which constitutes a key point regarding the adoption of fuel cells at a large scale.

Regarding electrocatalytic activity assessment, the redox competition (RC) mode of SECM, introduced by W. Schuhmann's group in 2006, is a recognised reference protocol[21]. It consists in polarizing the probe and the substrate in such a way that the same reaction occurs on both sides: the probe then evaluates the local reactant depletion due to its consumption by the electroactive sample (as shown in Figure 1). A scan over the surface thus reveals the local activity variations.

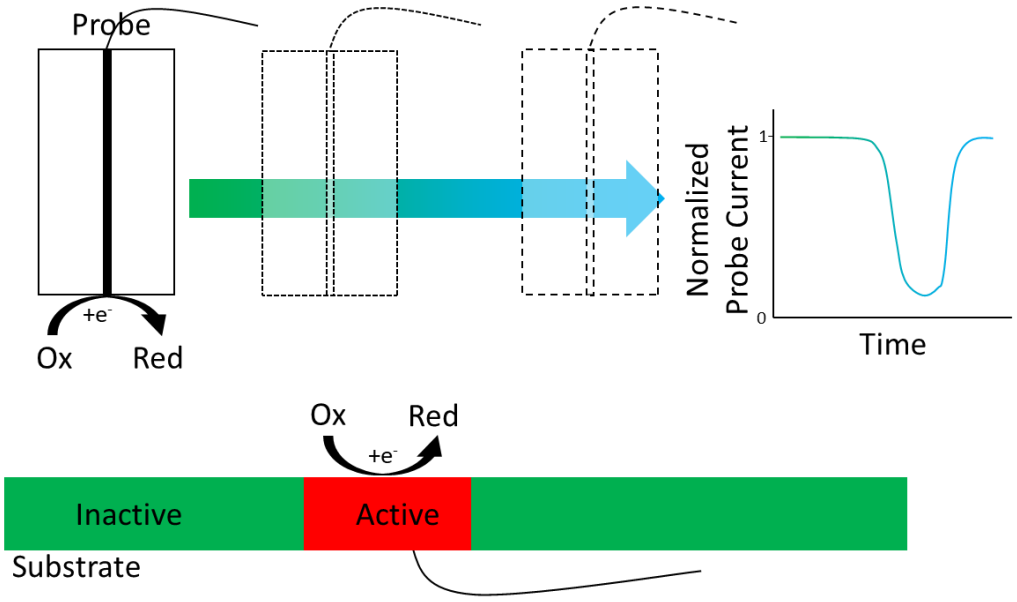

Figure 1. Scheme of the RC-SECM mode.

RC mode has already been used to visualize the cell breathing[22], to understand corrosion mechanism on CrN film[23], to study the consumption of oxygen from zinc oxide formation[24] or even to determine more accurately enzymatic kinetics[25] thanks to previous modelling studies of such a system[26]. For ORR catalysts, it operates in such a way that the scanning electrode is used as a probe of the local O_2 concentration[18,21,27]. However, the use of the technique still remains mostly limited to the SECM community, where studies are usually proof of concepts. We foresee that the expansion of the technique to quantitative studies could provide better knowledge of many catalysts that are currently being investigated within the context of the energetic transition. In fact SECM, and RC-SECM in particular, are presently underused by the community, in comparison to the benefits the technique can provide, namely its high resolution[28,29].

The lack of a comfortable configuration that would enable better ease and reproducibility, and particularly in complex conditions such as in acidic media to be compatible with PEMFC technology, is a key obstacle to the development of the RC mode approach. Herein, we show how the choice of the probe and substrate materials can help to stabilize the experimental configuration and enable steady state measurements while scanning the surface.

Up to now, Pt microelectrodes are the most frequently used for the RC mode[18,21,27,30], which is a rational choice considering the established electrocatalytic activity of this material towards ORR. However, Pt presents some drawbacks, for instance measurement instabilities are common at high probe current densities, and further it displays a high sensitivity to impurities that might be present in the solution. Subsequent alternatives such as the use of potential pulses[31] or high scan speeds[27] are required, but that may significantly hinder quantitative studies. On the other hand, gold as a probe metal has been used for other SECM measurements[16], but –to the best of our knowledge- not for ORR detection. Here, we show that the low catalytic activity of gold is not an issue for ORR detection, which makes it suitable for studying ORR in RC mode, and even in acidic media.

In theory, the high sensitivity of the RC mode enables the evaluation of very low catalytic activities, however in this case, the substrate activity is likely to enter in competition with the catalytic material[32]. Overall ORR studies are usually performed using glassy carbon (GC) substrate[30,33,34]. Boron doped diamond (BDD) catalytic activity toward ORR has been investigated[35], as other carbon based materials[36]. Furthermore, BDD has been used in SECM as a probe[37] or a studied material[35,38], but not as substrate for ORR catalytic activity determination. BDD has shown higher overpotential for ORR, higher stability and lower H_2O_2 production in acidic media compared to other carbon based substrates[39]. Here we demonstrate that BDD is an interesting alternative to standard carbon based substrates. We compared it to a GC substrate, due to its high representation in the literature, and a Si-wafer substrate covered with gold, as it is easy to produce, with good reproducibility and permits to achieve highly flat surface. The catalyst used to illustrate the potentiality of the new setup is a noble-metal free material based on carbon nanotubes (CNT) annealed with cobalt and nitrogen precursors[40].

Experimental

Materials

All chemicals and solvents of research grade were purchased in the highest purity from Sigma Aldrich and used as received. All gases (nitrogen, oxygen) were of 99.995% purity. Commercial grade NC3100 (purity >95%) multi-wall carbon nanotubes were obtained from Nanocyl (Belgium).

BDD substrate preparation

BDD was grown onto highly doped 4 inches silicon substrates by microwave plasma enhanced chemical vapor deposition (MPECVD) technique in a Seki Diamond AX6500 diamond growth reactor in a hydrogen plasma containing 1% methane as the source of carbon and trimethylboron as dopant. The resulting boron doping level is approximately $2x10^{21}$ cm^{-3} as determined by secondary ion mass

spectrometry measurements. The polycrystalline diamond film obtained is approximately 1 micron thick.

BDD substrate cleaning process

BDD substrates were immerged into a piranha solution during 30 minutes and then in pure H_2SO_4 at 300°C for 30 minutes. Afterward, KNO_3 was added into the solution until a yellow coloration started to appear and the substrates stayed still 30 minutes more in the 300°C solution. Then, the substrates were rinsed into a 300°C pure H_2SO_4 solution during 10 minutes and finally rinsed with distilled water.

In the case there was any doubt of catalyst residual traces on the substrate, a micro-wave hydrogen plasma exposure of the BDD surface, at a temperature of 600°C, was used to perform a complete reclaim of the BDD native surface.

Gold substrate preparation

Gold substrates were obtained by vacuum evaporation in a Balzers BAK 600 evaporator: a thin interlayer of chromium (to enhance gold adhesion on glass) and pure gold (99.99 % from Williams Advanced Materials) were evaporated at room temperature on silicium wafers. Prior to evaporation, the silicium wafers were rinsed 10 min under ultrasonication in water, ethanol and acetone successively. The thickness of the deposited layers was 3 nm of chromium and 30 nm of gold monitored in-situ by using a quartz crystal microbalance.

Catalyst preparation

The catalyst was prepared as described previously[40]. Briefly, $Co(NO_3)_2.6H_2O$, multi-wall carbon nanotubes (MWNTs) and triazolopyridine (TAPy) were mixed in ethanol and sonicated for 30 minutes. Ethanol was removed under low pressure and the black Co-TAPy/CNTs powder was pyrolyzed at 950°C during 2h under argon. This catalyst will be called Co-N-NTC.

Catalyst deposition

The catalyst ink was prepared by dispersing Co-N-NTC powder (20 mg) with 5% in wt of D-520 Nafion in ethanol (1 mL) under sonication (30 min) with a cup-horn coupled with a Vibra-Cell (VCX 130 PB from Sonics Material). Afterwards, the total volume is increased with ethanol to 2 mL and the process is repeated. The same process continues by increasing the total volume to 5/10/20/50/100/200 mL to obtain a catalyst ink of 0.1 $g.L^{-1}$.

The catalyst spot was obtained by two methods. The first one consists of dropping 2 mL of the catalytic ink onto the substrate heated at a temperature of 100°C with a micropipette. The second method uses the ExactaCoat apparatus from Sono-Tek to pulverize the solution onto the substrate. A mask with

144 micropatterns (from Micron Laser Technology) was used to obtain a controlled square spot in size and
145 volume of solution deposited.

146 Instrumentation

147 AFM and SEM measurements

148 AFM images were performed on a Veeco Dimension 3100 equipped with a Nanoscope IIIa controller
149 and analysed with the software Gwyddion. SEM images were recorded with a Hitachi S-4500 scanning
150 electron microscope.

151 Electrochemical measurements

152 Electrochemical measurements were performed in sulfuric acid (Sigma Aldrich). The gold and platinum
153 microelectrodes from Sensolytics had an active radius of 5 microns and a RG (the ratio between the
154 inactive part radius and the active part radius of the probe) of 30. SECM experiments were performed
155 on a modified M470 SECM Workstation from Bio-Logic Science Instruments. A four-electrode setup
156 was used for the SECM experiments. It involved a platinum or a gold microdisk as first working
157 electrode, a GC, a gold or a BDD substrate as second working electrode, a saturated calomel electrode
158 (SCE) as reference and a net made of platinum wires as counter electrode. Both reference and counter
159 electrodes are placed in sintered guards to avoid direct contact between the analysed solution, the
160 reference and the counter electrodes. The probe-substrate distance was evaluated by approaching the
161 probe in the vicinity of the area of interest, somewhere without catalyst, and by letting the substrate
162 at open circuit potential (OCP). In this case a negative feedback was obtained, and a comparison with
163 theory provides the relationship between the probe position and the probe-substrate distance[41,42].
164 Unless mentioned, the analysis of the ORR activity was made in H_2SO_4 0.1 M solution. The probe was
165 stabilized 300 s before each measurement.

166 Results & discussion

167 The working electrodes are central to the SECM technique. Improving both of them to specific
168 demands allows progresses in the quality of measurements. First, in order to investigate the first
169 working electrode, i.e. the probe, a linear sweep voltammetry (LSV) is performed from OCP up to the
170 solvent reduction signal, in Ar saturated solution and O_2 saturated solution. At this step, the probe is
171 put in solution without the substrate to avoid any interaction.

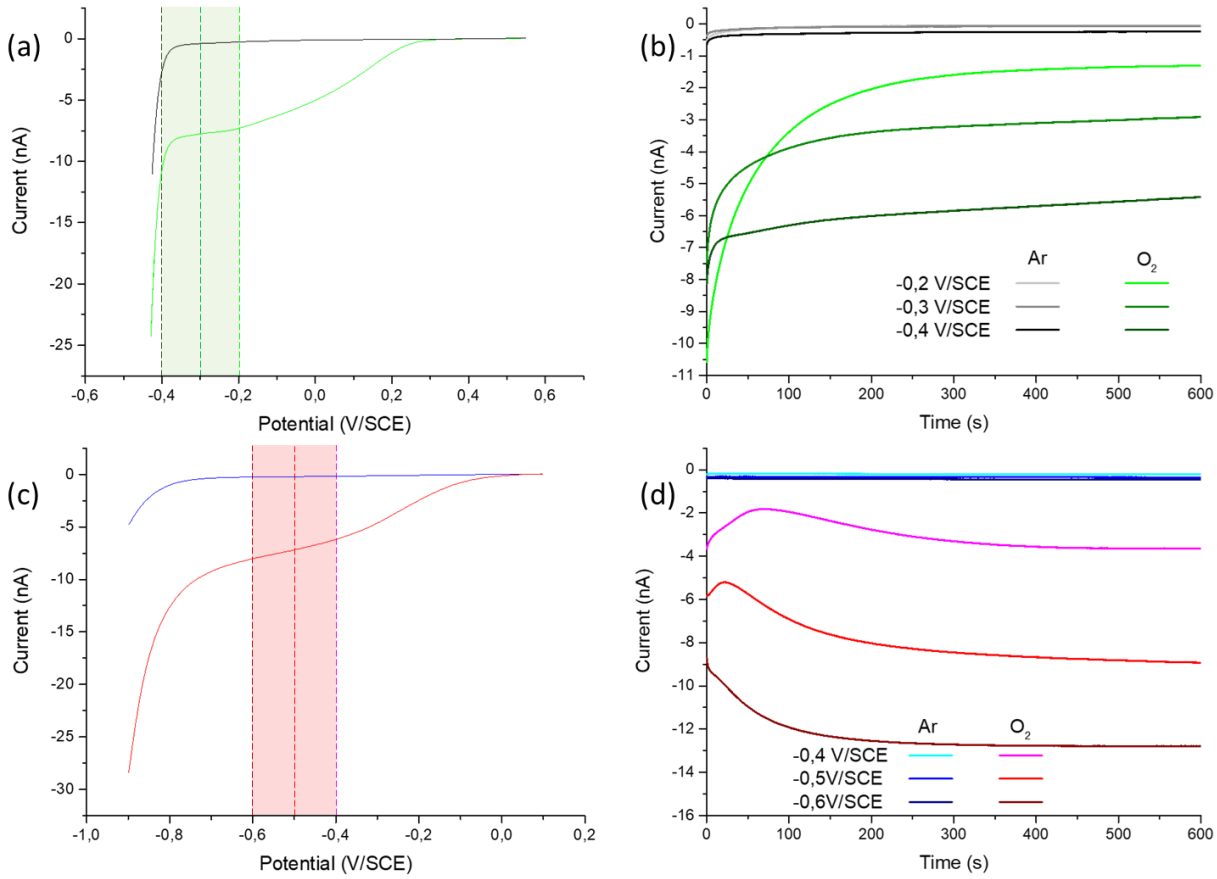

Figure 2. (a) LSV at the platinum probe from 0.55 to -0.43 V/SCE with a 10 mV/s scan rate. (b) CA at the platinum probe at different potentials (-0.2, -0.3 and -0.4 V/SCE). Black curves for Ar saturated solution and green curves for O_2 saturated solution in (a & b). (c) LSV at the gold probe from 0.1 to -0.9 V/SCE with a 10 mV/s scan rate. (d) CA at the gold probe at different potentials (-0.4, -0.5 and -0.6 V/SCE). Blue curves for Ar saturated solution and red curves for O_2 saturated solution in (c & d). All measurements were made in H_2SO_4 0.1M, r_T = 5 µm and RG = 30 for both probes.

As shown in Figure 2.a, a well-defined plateau is observed between -0.2 to -0.4 V/SCE for the ORR at the platinum probe, illustrated by the green bar. Several potentials of this plateau are then tested by chronoamperometry (CA). Each potential is applied for 600 seconds, in order to investigate the stability of the measurement. The probe is polished and cleaned between each measurement and the procedure is repeated several times in the O_2 saturated solution. The results presented Figure 2.b show the currents measured at -0.2, -0.3 and -0.4 V/SCE. For the three potentials, an exponential loss of current is observed, followed by a stabilization of the slope to a non 0 value. This behaviour is not the one expected from a well-defined diffusion plateau as observed on the CV. Furthermore, the current variation during the first 200 seconds is not exclusively due to the establishment of the diffusion profile in the vicinity of the probe, as this is a process that has time constant of typically seconds[43]. It is also related to the evolution of platinum surface states, with possibly some contamination due to side reactions. Furthermore, the current densities are not the same along the probe surface increasing the complexity of such phenomenon. In any case, the observation is in accordance with what is observed

in the literature[21]. In any case, the important element for SECM imaging is to have a steady-state current at the probe. The Pt probe current was the most stabilized after 300s with a linear loss of current. After this stabilization step, the sensitivity, the detection threshold and the instability can be then evaluated. These values are shown in Table 1. We evaluated the theoretical sensitivity by using the equation of the current at a diffusion plateau[44]. In the equation 1, n is the number of electrons exchanged (4 in the case of a complete O_2 reduction), F is the Faraday constant, D_0 is the diffusion coefficient of O_2 in H_2SO_4 ($1.4x10^{-5}$ $cm^2.s^{-1}$ for 0.5M)[45], C_0 is the concentration of O_2 in H_2SO_4 (in the case of an O_2 saturated H_2SO_4 0.1M solution, it is $1.27x10^{-6}$ $mol.cm^{-3}$ at 298K)[46] and r_T is the radius of the active part of the electrode. The theoritical sensitivity is 10.8 nA/mM(O_2). The sensitivity measured at t_{600} is 1.0, 2.2 and 4.3 nA/mM(O_2) for -0.2, -0.3 and -0.4 V/SCE respectively, which are significantly lower values compared to the theoritical one. It can be noticed that the sensitivity measured at t_0 is 8.3, 5.9 and 6.4 respectively which is closer to the theoritical one.

$$I = 4nFD_O C_O r_T \quad (1)$$

We decided to consider the detection threshold as the O_2 concentration for a current equal to the current measured in absence of O_2 in solution. This is calculated by the equation 2 where I_{O_2} is the current measured in the O_2 saturated solution and I_{Ar}, the current measured in the Ar saturated solution. For -0.2, -0.3 and -0.4 V/SCE, the detection threshold is 47, 31 and 46 µM(O_2) respectively.

$$Detection\ threshold = \frac{C_O}{I_{O_2} \times I_{Ar}^{-1}} \quad (2)$$

Besides, the instability of the measurement is evaluated by considering the current difference between 480 and 600 s to have a well-defined slope compared to 300 s where the stabilization occurs (see equation 3, where I_{600} is the current at t_{600}, I_{480} is the current at t_{480} and I_m is the averaged current between t_{480} and t_{600}).

$$Instability = \left| \frac{I_{600} - I_{480}}{t_{600} - t_{480}} \times \frac{1}{I_m} \right| x100 \quad (3)$$

The calculated instability is expressed in %/min which corresponds to the current percentage loss every minute of the measurement. In the case of the Pt probe, the instability is 0.44, 0.62 and 0.44 for -0.2, -0.3 and -0.4 V/SCE respectively.

Exactly the same procedure is applied to the gold probe. The LSV and the CA are presented in Figure 2.c and Figure 2.d respectively. In this case, a pseudo-plateau between -0.4 to -0.7 V/SCE is observed (illustrated by the red bar) in the ORR window instead of a well-defined diffusion plateau. Different CA were done in the same condition as previously for the platinum probe, except that the chosen potentials are -0.4, -0.5 and -0.6 V/SCE, in accordance with the observed lower electrocatalytic activity

of gold versus platinum. Here also, stabilisation of measurements lasted about 300 s. The shape of the current curves is different in the case of gold. Here again, the probe's surface state impacts positively or negatively the kinetics at the surface. The difference between Pt and Au probes can be explained by their different ORR mechanisms occurring at the surface, as well as the difference in the stability of the surface states. It can be noticed in the Figure 2.d that the stabilized current is close to the starting current. Thus, for the gold probe, the sensitivity calculated is 3.3, 7.4 and 10.0 nA/mM(O_2) for -0.4, -0.5 and -0.6 V/SCE respectively. The detection threshold is 63, 49 and 46 µM(O_2) and the instability is 0.62, 0.13 and 0.19 %/min respectively. The sensitivity at -0.6 V/SCE is close to the theoretical one. As an additional advantage, the use of a gold probe permits to avoid the possibility to contaminate the substrate with a highly active material such as platinum. Moreover, the stability of the current at the gold probe allows long time acquisition with steady-state measurements. Therefore, based on the comparison of their sensitivities, their detection thresholds and their instabilities between platinum and gold probes, the latter really appears as a very interesting alternative probe for studying ORR.

Table 1. Averaged values from the CA at the probes at t_{600s} and calculated sensitivity, detection threshold and instability for these values.

Active part composition	E_{probe} (V/SCE)	Current at t_{600s} (nA) Ar_{sat}	Current at t_{600s} (nA) O_{2sat}	Sensitivity (nA/mM(O_2)	Detection threshold (µM(O_2))	Instability (%/min)
Platinum probe	-0.2	-0.04	-1.22	1.0	46	0.44
	-0.3	-0.07	-2.83	2.2	31	0.62
	-0.4	-0.20	-5.48	4.3	46	0.44
Gold probe	-0.4	-0.21	-4.27	3.3	63	0.62
	-0.5	-0.36	-9.39	7.4	49	0.13
	-0.6	-0.46	-12.72	10.0	46	0.19

The supporting substrate used to analyse the activity of a catalyst is another important element for electrochemical measurements. Micrometric planarity, roughness and electrochemical activity are key parameters that influence the analysis. Figure 3 shows AFM (a) and SEM (b) images of a BDD substrate, where one can observe its polycrystallinity. The roughness average (Ra) and the root-mean-square roughness (Rq) of BDD is measured by AFM and is 39.9 nm and 50.0 nm respectively. Moreover, the maximum measured height is 372 nm. In the present work, a micrometric probe is used, and the positioning is performed at the micrometric scale (typically 30 microns, as shown Figure 5), so the ~100 nm roughness of the sample is negligible[49]. Besides, the use of a Si-wafer as substrate support guaranties a negligible non-planarity of the whole sample. Thus, the topography of the BDD substrate is highly acceptable for the investigation of micrometric spots of catalysts with the RC-mode and a micrometric probe.

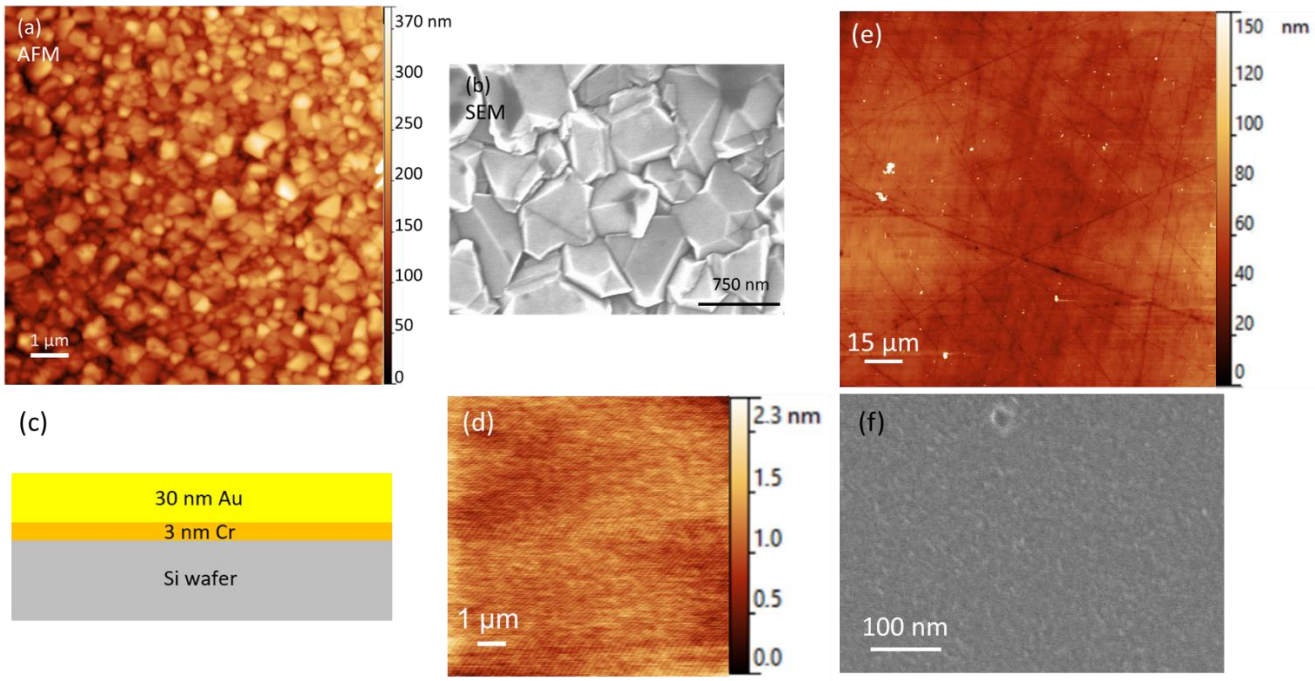

Figure 3. (a) AFM image showing a thickness of 372 nm, Ra of 39.9 nm and Rq of 50.0 nm and (b) SEM image showing crystals smaller than 1 µm in diameter of a BDD substrate. (c) Scheme of the gold substrate structure. (d) AFM image showing a 2.3 nm thickness, Ra of 178 pm and Rq of 225 pm of a gold substrate. (e) AFM image showing a GC substrate with a Ra of 7.2 nm and a Rq of 11.4 nm. (f) SEM image of a GC substrate.

As an alternative to BDD, a Si-wafer covered with gold and a GC substrate can be considered. The gold substrate structure is illustrated in Figure 3.c and d for the AFM image. The maximum measured height is 2.3 nm with a Ra of 178 pm and a Rq of 225 pm which allows to scan on a nanoscale surface where inhomogeneities come from the investigated material only. The AFM and SEM image of a GC substrate are presented in Figure 3.e and f respectively. The maximum height measured on the GC substrate is almost 650 nm despite a Ra of 7.2 nm and a Rq of 11.4 nm. The average value is 58.3 nm meaning there is scarce but important inhomogeneities on the GC substrate. The polishing process of the GC substrate is of the outmost importance to allows a high planarity and so nanoscale measurements on it. In contrary, gold and BDD substrates, thanks to the Si-wafer support, keep their planarity on the whole surface.

Electrochemical results are presented Figure 4 comparing BDD to a GC substrate, a gold substrate and a catalyst spot of Co-N-NTC deposited on BDD. The samples are studied by RC-SECM at a constant height with a probe-substrate distance of 50 µm. The process involved is presented Figure 4.A and is done in acidic media saturated with oxygen (H_2SO_4 0.1 M) due to the acidic condition used in a PEMFC.

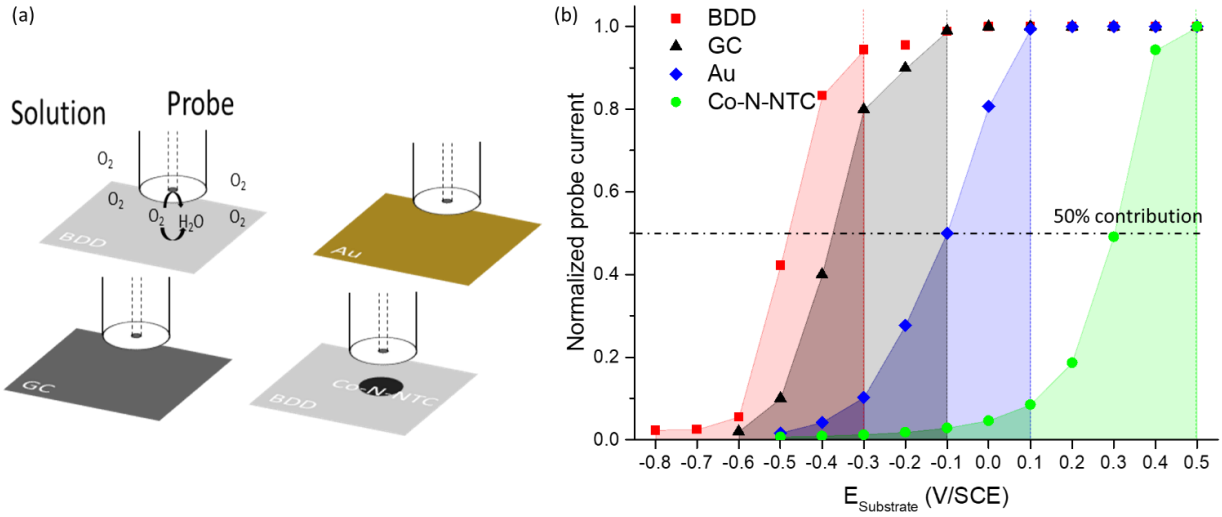

Figure 4. (a) Scheme presenting the process involved in the RC-SECM measurement to analyse the ORR activity of BDD, GC, Au and the catalyst spot. (b) Results of chronoamperometry (CA) at different substrate potentials with a gold probe (r_T = 5 µm, RG = 30, E_{probe} = -0.6V/SCE) in H_2SO_4 0.1 M solution saturated with oxygen and with a distance probe-substrate of 50 µm. Measurements are made on a clean BDD substrate (■), a clean GC substrate (▲), a clean gold substrate (♦) and a Co-N-NTC spot (●). The area under the curves represent the potential zone were the competition between the probe and the substrate occurs.

The probe was held at -0.6 V/SCE in order to reduce O_2 during all measurements. Samples were held at different potentials, from one from which the sample is inactive, to one corresponding to a high activity of the sample (almost no current at the probe) with a 100 mV difference between each measurement. Each potential was held at least 100 s for the current to reach a plateau once stabilized. The results of the experiment are presented in Figure 4.b.

The competition starting point between the probe and the samples is noticed at a potential between 0.5 and 0.4 V/SCE for the Co-N-NTC spot, 0.1 V/SCE for the gold substrate, between -0.1 and -0.2 V/SCE for the GC substrate and -0.3 V/SCE for the BDD substrate. This means that the competition occurs for more negative potentials applied to the substrate than the one of this starting point. A 50 % contribution of samples is observed at 0.3 V/SCE for the Co-N-NTC spot, -0.1 V/SCE for the gold substrate, -0.41 V/SCE for the GC substrate and -0.48 V/SCE for the BDD substrate. Finally, the probe measures a current almost null at -0.2 V/SCE for the Co-N-NTC spot, -0.5 V/SCE for the gold substrate and -0.7 V/SCE for the BDD. However, for the GC substrate, even at the lowest potentials, the probe current was not null. This can be explained by an uncomplete ORR at the GC substrate. These results showed that the BDD substrate is less active than the other substrates. Moreover, according to previous investigations made for GC through cyclic voltammetry, the same conclusion was established in acidic[39] and alkaline media[50].

Overall, the large inactive window of BDD -until -0.3 V/SCE no contribution from the substrate is observed- offers a wider range of experimental conditions that can be used, as illustrated with the Co-N-NTC spot with a loading around 200 µg/cm^2. There, the O_2 consumption by the catalyst is total before the O_2 consumption starts at the substrate, which is not the case with gold. This proves that much lower electrocatalytic activities or loadings can be investigated with BDD.

In order to further show that gold probe and BDD substrate are suitable to perform SECM imaging at steady state, Figure 5.a shows a 3 mm² optical image of two Co-N-NTC spots of 120 (a) and 230 (b) µg/cm² sprayed with the ExactaCoat system through a micro-patterned mask to obtain this well-defined square spots. The RC-SECM image of these spots is shown in Figure 5.b at $E_{substrate}$ = -0.3 V/SCE. The full RC-SECM image (with both forward and backward scans) is recorded within 2 hours.

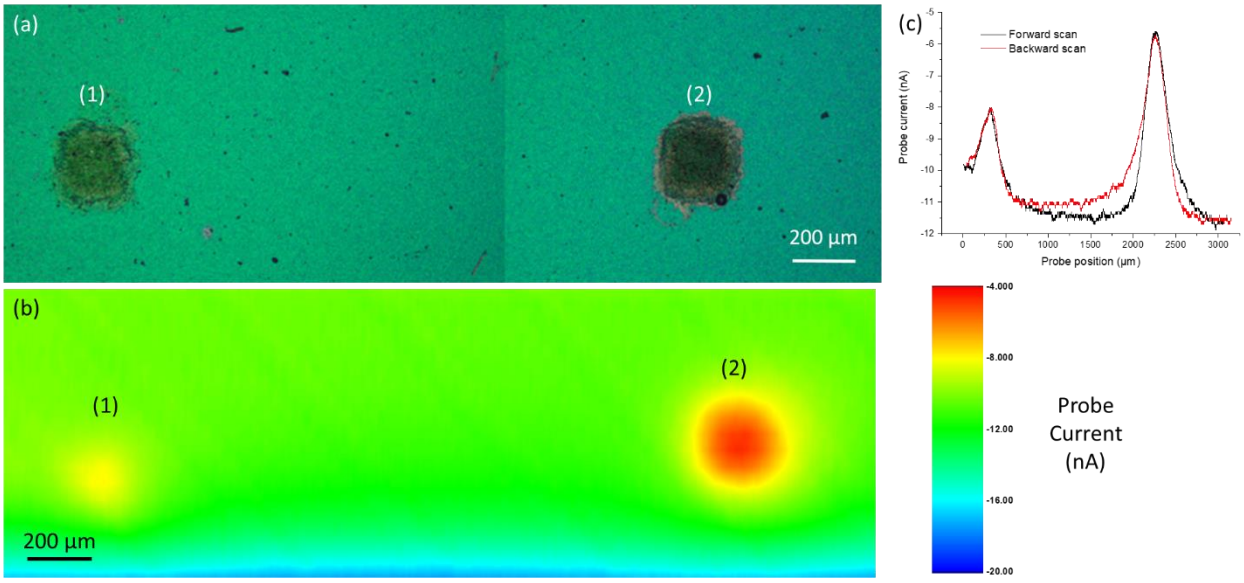

Figure 5. (a) Optical image of (1) 120 µg/cm² and (2) 230 µg/cm² Co-N-NTC spots on a BDD substrate. (b) RC-SECM image of the spots shown in (a). (c) RC-SECM forward (black curve) and backward (red curve) linescans at Y = 450 µm from the RC-SECM image (b) corresponding. SECM experiments done with a gold probe (r_T = 12 µm, RG = 11, E_{probe} = - 0.45V/SCE) in H_2SO_4 0.1 M solution saturated with oxygen and with $E_{substrate}$ = -0.3 V/SCE, a distance probe-substrate of 30 µm and v_{scan} = 20 µm/s.

As shown in Figure 5.c, forward and backward linescans overlap above the active spot, and this proves the steady state nature of the measurement. Still, non-stationarity can be seen when the probe is at the extremity of the spots, and in this case the current is smaller if the probe is approaching the center of the spot, and larger in the contrary. This fits the expectations, and does not affect the maximal current variation, which is the most important parameter regarding the spot electrocatalytic activity evaluation. At each line of the image, the current obtained far from the spots can be used to calibrate the relationship between the measured current and the oxygen concentration, by evaluating the effective number of electrons transferred:

$$n = \frac{I}{4FD_O C_O r_T \beta(RG) NiT(L,RG)} \quad (4)$$

with $\beta(RG)$, a correction factor due to the enhancement of diffusion limiting current for the small RG values[51] and NiT(L, RG), a correction factor due to diffusion hindering similar than a negative feedback[42]. With the experimental conditions of Figure 5.c (RG = 11, L = 2.5; L being the ratio between the distance probe-substrate with the r_T), $\mathrm{NiT(L, RG)} = 0.79$ so n= 1.8 with the current measured at the end of the linescan (-11.5 nA) presented Figure 5.c. Alternatively, $\mathrm{NiT(L, RG)}$ = 0.78 is the ratio between the current measured far from the spot, divided by the current measured in solution. n is smaller than 2 here probably because the diffusion plateau is not reached at the working potential.

This way, the quantification of the oxygen consumption rate will become possible. It will need the support of numerical simulation, explicitly taking into account the experimental parameters such as the probe-to-substrate distance, the probe size (active and inactive part), and the spot size and shape. This is fully justified in a context of performing the benchmarking of catalysts, which will be done in future works.

Conclusion

Herein, we showed how steady state evaluation by RC-SECM for ORR detection in acidic conditions can be achieved with gold probes and BDD substrates. The gold probe exhibited a remarkable current stability, with variation values under 0.2 % variation per minute), further to a good sensitivity and a detection threshold similar to that of the platinum probe. Similarly, we also demonstrated that BDD as supporting substrate shows a very large inactivity window, up to -0.3 V vs SCE, with a submicrometric roughness and a small long-distance non-planarity, thanks to the Si-wafer support underneath. The same setup can also be considered for alkaline media investigations. This may be the basis of future works. Furthermore, preparation of flat BDD substrates is also planned in the future.

Conflicts of interest

The authors have no conflict of interest to declare.

Acknowledgement

The authors acknowledge the SENTINEL project, funded by the European Union's Horizon 2020 research and innovation program under the Marie Sklodowska-Curie grant agreement no 812398, and the PEGASUS project, funded by the European Union's Horizon 2020 research and innovation program FCH-01-2-2017, no779550.

344

345

346

References

[1] J. Heinze, *Angew. Chemie Int. Ed. English*, **1993**, 32, 1268–1288.

[2] A. Dobrzeniecka *et al.*, *Catal. Today*, **2013**, 202, 55–62.

[3] A. S. Arico, P. Bruce, B. Scrosati, J. M. Tarascon, and W. Van Schalkwijk, *Nat. Mater.*, **2005**, 4, 366–377.

[4] Y. Yu, T. Sun, and M. V. Mirkin, *Anal. Chem.*, **2015**, 87, 7446–7453.

[5] C. M. Sánchez-Sánchez, J. Rodríguez-López, and A. J. Bard, *Anal. Chem.*, **2008**, 80, 3254–3260.

[6] A. Minguzzi, M. A. Alpuche-Aviles, J. R. Lopez, S. Rondinini, and A. J. Bard, *Anal. Chem.*, **2008**, 80, 4055–4064.

[7] J. J. Santana, J. Gonzalez-Guzman, L. Fernandez-Merida, S. Gonzalez, and R. M. Souto, *Electrochim. Acta*, **2010**, 55, 4488–4494.

[8] J. Y. Kim, H. S. Ahn, and A. J. Bard, *Anal. Chem.*, **2018**, 90, 3045–3049.

[9] A. Domenech-Carbo *et al.*, *Electrochim. Acta*, **2014**, 115, 546–552.

[10] A. Domenech-Carbo, M. Teresa Domenech-Carbo, M. Lastras Perez, and M. Herrero-Cortell, *Forensic Sci. Int.*, **2015**, 247, 79–88.

[11] J. Hui, M. Burgess, J. Zhang, and J. Rodriguez-Lopez, *ACS Nano*, **2016**, 10, 4248–4257.

[12] K. C. Huang *et al.*, *J. Mater. Chem.*, **2011**, 21, 10384–10389.

[13] A. Sumboja, U. M. Tefashe, G. Wittstock, and P. S. Lee, *J. Power Sources*, **2012**, 207, 205–211.

[14] Z. Wang, Y. Liu, and V. M. Linkov, *J. Power Sources*, **2006**, 160, 326–333.

[15] A. Kishi, M. Inoue, and M. Umeda, *J. Phys. Chem. C*, **2010**, 114, 1110–1116.

[16] J. L. Fernández, D. A. Walsh, and A. J. Bard, *J. Am. Chem. Soc.*, **2005**, 127, 357–365.

[17] W. Li, F.-R. F. Fan, and A. J. Bard, *J. Solid State Electrochem.*, **2012**, 16, 2563–2568.

[18] S. Kundu *et al.*, *J. Phys. Chem. C*, **2009**, 113, 14302–14310.

[19] S. Kumar, P. K. Sahoo, and A. K. Satpati, *ACS Omega*, **2017**, 2, 7532–7545.

[20] G. J. Lu, J. S. Cooper, and P. J. McGinn, *Electrochim. Acta*, **2007**, 52, 5172–5181.

[21] K. Eckhard, X. Chen, F. Turcu, and W. Schuhmann, *Phys. Chem. Chem. Phys.*, **2006**, 8, 5359–

5365.

[22] M. Nebel, S. Grützke, N. Diab, A. Schulte, and W. Schuhmann, *Faraday Discuss.*, **2013**, 164, 19–32.

[23] S. Gao, C. Dong, H. Luo, K. Xiao, X. Pan, and X. Li, *Electrochim. Acta*, **2013**, 114, 233–241.

[24] S. Thomas *et al.*, *J. Appl. Electrochem.*, **2014**, 44, 747–757.

[25] I. Morkvenaite-Vilkonciene, A. Ramanaviciene, P. Genys, and A. Ramanavicius, *Electroanalysis*, **2017**, 29, 1532–1542.

[26] F. Ivanauskas, I. Morkvenaite-Vilkonciene, R. Astrauskas, and A. Ramanavicius, *Electrochim. Acta*, **2016**, 222, 347–354.

[27] A. J. Wain, *Electrochim. Acta*, **2013**, 92, 383–391.

[28] P. Sun and M. V Mirkin, *Anal. Chem.*, **2006**, 78, 6526–6534.

[29] B. B. Katemann, A. Schulte, and W. Schuhmann, *Electroanalysis*, **2004**, 16, 60–65.

[30] A. Tiwari, V. Singh, D. Mandal, and T. C. Nagaiah, *J. Mater. Chem. A*, **2017**, 5, 20014–20023.

[31] X. X. Chen, A. J. R. Botz, J. Masa, and W. Schuhmann, *J. Solid State Electrochem.*, **2016**, 20, 1019–1027.

[32] T. Löffler, P. Wilde, D. Öhl, Y. T. Chen, K. Tschulik, and W. Schuhmann, *Faraday Discuss.*, **2018**, 210, 317–332.

[33] B. Lim *et al.*, *Science (80-.).*, **2009**, 324, 1302–1305.

[34] L. Qu, Y. Liu, J. Baek, and L. Dai, *ACS Nano*, **2010**, 4, 1321–1326.

[35] V. S. Dilimon, N. S. V. Narayanan, and S. Sampath, *Electrochim. Acta*, **2010**, 55, 5930–5937.

[36] G. Wu and P. Zelenay, *Acc. Chem. Res.*, **2013**, 46, 1878–1889.

[37] K. B. Holt, J. Hu, and J. S. Foord, *Anal. Chem.*, **2007**, 79, 2556–2561.

[38] S. Tan *et al.*, *Phys. Chem. Chem. Phys.*, **2017**, 19, 8726–8734.

[39] M. Gara and R. G. Compton, *New J. Chem.*, **2011**, 35, 2647–2652.

[40] A. Morozan, P. Jégou, B. Jousselme, and S. Palacin, *Phys. Chem. Chem. Phys.*, **2011**, 13, 21600–21607.

[41] B. R. Horrocks, M. V. Mirkin, and A. J. Bard, *J. Phys. Chem.*, **1994**, 98, 9106–9114.

[42] R. Cornut and C. Lefrou, *J. Electroanal. Chem.*, **2007**, 608, 59–66.

[43] M. V. Mirkin and S. Amemiya, Nanoelectrochemistry, in *CRC Press*, CRC Press, 2015, 439–461.

[44] K. Aoki and J. Osteryoung, *J. Electroanal. Chem. Interfacial Electrochem.*, **1981**, 122, 19–35.

[45] J. J. Salvador-Pascual, S. Citalán-Cigarroa, and O. Solorza-Feria, *J. Power Sources*, **2007**, 172, 229–234.

[46] T. N. Das, *Ind. Eng. Chem. Res.*, **2005**, 44, 1660–1664.

[47] Y. Shen, M. Trauble, and G. Wittstock, *Anal. Chem.*, **2008**, 80, 750–759.

[48] A. M. Gómez-Marín, A. Boronat, and J. M. Feliu, *Russ. J. Electrochem.*, **2017**, 53, 1029–1041.

[49] F. O. Laforge, J. Velmurugan, Y. Wang, and M. V Mirkin, *Anal. Chem.*, **2009**, 81, 3143–3150.

[50] T. Yano, D. A. Tryk, K. Hashimoto, and A. Fujishima, *J. Electrochem. Soc.*, **1998**, 145, 1870–1876.

[51] C. Lefrou and R. Cornut, *ChemPhysChem*, **2010**, 11, 547–556.

Table of Contents

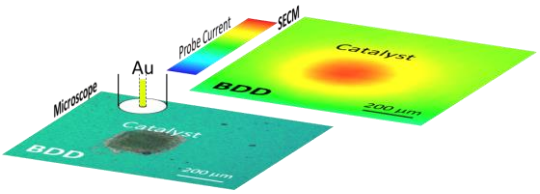

This paper demonstrates how a judicious choice of probe and substrate materials opens up improved performances to achieve steady state measurements, in this case, for oxygen reduction reaction (ORR) catalytic activity detection through the redox competition scanning electrochemical microscopy (RC-SECM).

We show that the use of gold enhances the stability of the local oxygen concentration detection in comparison to the regularly used platinum one. We evaluate boron doped diamond as an appealing support substrate, that shows a low ORR activity, high stability and very good reusability.

Keywords

Boron doped diamond; Electrocatalysis; ORR; Redox competition mode; SECM